# Interaction of water with oligo(ethylene glycol) terminated monolayers: wetting *versus* hydration†

Mustafa Sayin,[a] Alexei Nefedov [b] and Michael Zharnikov *[a]

Biorepulsivity of oligo(ethylene glycol) (OEG) substituted self-assembled monolayers (SAMs), serving as model systems for analogous polymeric surfaces, is generally ascribed to the hydration effect. In this context, we applied temperature-programmed desorption to study interaction of water ($D_2O$) with a series of OH-terminated, OEG-substituted alkanethiolate SAMs with variable length of the OEG strand, defining their biorepulsion behavior. Along with the ice overlayer (wetting phase), growing also on the surface of the analogous non-substituted films, a hydration phase, corresponding to the adsorption of $D_2O$ into the OEG matrix, was observed, with a higher desorption energy (12.4 kcal $mol^{-1}$ *vs.* 10.4 kcal $mol^{-1}$) and a weight correlating with the length of the OEG strand and, consequently, with biorepulsivity. The formation of hydration phase was found to occur over an activation barrier, presumably by temperature-promoted diffusion from the wetting phase, with this process being additionally enforced by a pre-desorption annealing.

## Introduction

Interaction of biomolecules and biological fluids with organic and inorganic materials is a crucially important issue in context of modern biophysical chemistry, biotechnology, and medicine. A particular interesting phenomenon in this context is antifouling behavior (termed also as biorepulsivity or ''inertness'') of some materials which exhibit only weak interaction with biomolecules and bioorganisms preventing their adsorption and settlement on the respective surfaces. A variety of such surfaces has been reported, including phosphocholine, polysaccharides, mannose-functionalised substrates, *etc.* The most popular and promising type of biorepulsive surfaces are, however, those, which are based on poly- or oligo(ethylene glycol)s (PEGs and OEGs, respectively).[1–6] These surfaces can be comprised of both polymeric materials[3] and OEG-substituted self-assembled monolayers (SAMs).[2,4–6] The latter films have essential advantages such as monodispersity and precise control of biorepulsion by the architecture of the SAM precursors and characteristics of their assembly.[4,5,7–9] Accordingly, they represent a suitable model playground to study biorepulsion in detail, giving additionally an insight into the physical and chemical factors behind this behavior which is not fully understood so far.

The most reasonable explanation of the biorepulsion behavior refers to interaction of the bioinert surfaces with water,[6,10] with the key factor being, presumably, hydration[6] which relies on the hydrogel-like character of the PEG and OEG compounds. In particular, for the immobilized PEG polymer films, the large gain in free energy upon hydration of these films is assumed to protect them against dehydration and compression by adsorbing biomolecules.[1,11] The entropy contribution associated with high conformational freedom of the polymeric chains plays then the most essential role.[1,11] This contribution is, however, much smaller in the case of densely packed OEG-substituted SAMs since the conformational freedom of the OEG moieties is largely restricted.[6,12] Different explanations of the biorepulsive properties have then been given, including (i) long-range electrostatic interaction between (charged) proteins and substrate, mediated by the negative charge of the hydrated OEG SAMs[13] and (ii) the formation of physically distinct interphase water adlayer on the surface of OEG-substituted SAMs, which results in the creation of ''solute-free'' exclusion zone preventing the irreversible adsorption of proteins.[6,10,14–17] These models are still heavily debated but the most likely explanation of the bioinertness of OEG-substituted SAMs is, similar to the polymer case (see above), their hydration, with the major effect provided, however, not by the entropy but by the large gain in free energy (mediated in this case by the enthalpy) upon hydration of the OEG moieties, protecting them against dehydration and compression by strongly adsorbing biomolecules and bioorganisms.[6]

[a] *Applied Physical Chemistry, Heidelberg University, Im Neuenheimer Feld 253, 69120 Heidelberg, Germany. E mail: Michael.Zharnikov@urz.uni heidelberg.de*
[b] *Institute of Functional Interfaces, Karlsruhe Institute of Technology (KIT), Hermann von Helmholtz Platz 1, 76344 Eggenstein Leopoldshafen, Germany*

† Electronic supplementary information (ESI) available. See DOI: 10.1039/d0cp00906g

The existence and exact character of the proposed hydration phase is, however, difficult to address experimentally, with such popular approaches as neutron reflectivity, infrared reflection absorption spectroscopy (IRRAS), atomic force microscopy, *etc.* providing, in the given case, a limited information only.[10,15,18,19] An alternative technique, which, to the best of our knowledge, has not been used in this context so far, is temperature-programmed desorption (TPD). In the case of SAMs, this technique has only been applied in context of wetting properties, dealing with adsorption and desorption of water on surfaces of specific wettability, such as $-CH_3$, –OH, $-CH_3$/–OH, $-CF_3$, $-C_6H_5$, (–C O)$OCH_3$, –COOH, and $-CH_3$/–COOH terminated alkanethiolate (AT) monolayers on Au(111).[20–23] Some of these studies were complemented by IRRAS experiments.[24–26] It was found that water adsorbs stronger on a polar than on a non-polar surface. At $T \approx 100$ K and a moderate coverage water mostly condenses in an amorphous ice phase, independent of the character of the organic substrate.[24–26] With increasing temperature, the amorphous ice crystallizes into a polycrystalline phase. The temperature of the structural transition is determined by the chemical properties of the surface. For extremely hydrophobic surfaces ($-CH_3$) this temperature is about 110 K, for hydrophilic surfaces (–OH), it is in a range of 140–150 K.[20,26] In addition, there are significant differences in morphology dependent on the character of the substrate: whereas ice clusters are nearly two-dimensional and flat on hydrophilic organic surfaces, they are three-dimensional and drop-like on hydrophobic surfaces.[20,26]

In view of the above reference data and potential importance of water for the bioinertness of PEG/OEG surfaces, we studied here adsorption a desorption of water ($D_2O$) onto a series of OEG-substituted AT SAMs on Au(111), *viz.* HS–$(CH_2)_{11}$–$(O–CH_2–CH_2)_n$–OH (EG*n*–OH; $n$ = 1, 3, 5, and 6) and HS–$(CH_2)_{11}$–$(O–CH_2–CH_2)_n$–$CH_3$ (EG*n*–OMe; $n$ = 3 and 6) monolayers as well as the reference HS–$(CH_2)_{11}$–OH (EG0–OH) and HS–$(CH_2)_{15}$–$CH_3$ (C16) films (Fig. 1). Significantly, the packing density of the EG*n*–OH SAMs is mainly determined by their AT part and is, therefore, nearly independent of the length of the OEG segment, which has been verified by us.[27] Also, the wetting properties of these films are almost independent of $n$,[5,7] which have been verified as well.[27] However, their inertness to protein adsorption and biofouling varies significantly over the series: whereas these films are not biorepulsive at small $n$, they become protein-repelling if their OEG part consists of more than two or three EG units,[7,9,10] which has been verified by us using fibrinogen as a test protein.[27] Thus, the EG*n*–OH SAMs represent an ideal model system with variable protein-repelling properties at an almost constant packing density and hydrophilicity, which both are similar to those of the reference EG0–OH film. In contrast, the EG6–OMe SAM, exhibiting the same biorepulsivity as the EG6–OH monolayer,[5] is more hydrophobic, in view of the terminal methyl group. This is a representative example of the fact that the wetting properties of OEG/PEG surfaces don't precisely correlate with their biorepulsive behavior, even though a certain correlation occurs.[5]

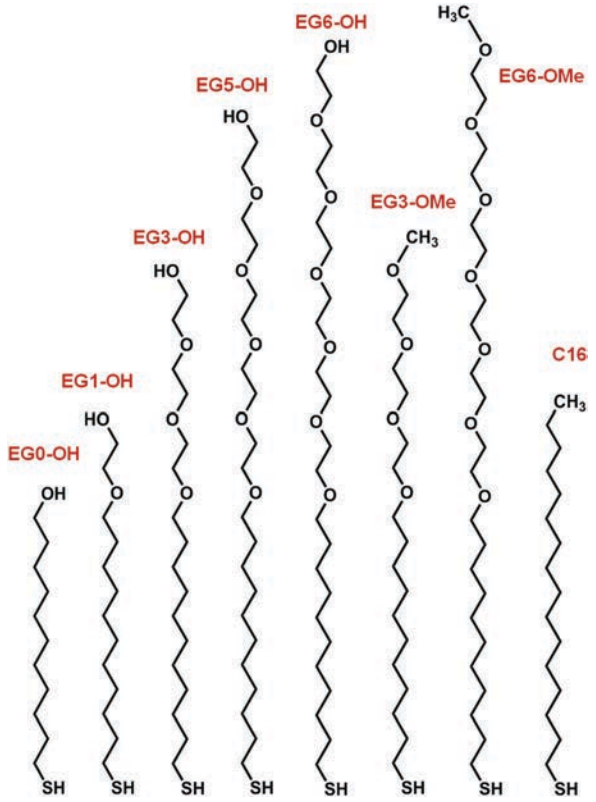


Fig. 1 A schematic drawing of the SAM forming molecules of the present study along with their acronyms.

## Experimental section

The EG*n*–OH and EG*n*–OMe precursors were purchased from ProChimia, Poland; the EG0–OH and C16 substances were purchased from Sigma-Aldrich. The gold substrates for the SAM preparation were purchased from Georg Albert PVD, Silz, Germany. They were fabricated by thermal evaporation of ~30 nm of gold (99.99% purity) onto polished single-crystal silicon (100) wafers (Silicon Sense) that had been precoated with a 9 nm titanium adhesion layer. The films were polycrystalline, with preferable (111) orientation. The SAMs were prepared according to the literature recipes,[7,9] by immersion of freshly prepared gold substrates into a 1 mmol solutions of the respective precursors in absolute ethanol for 24 h at room temperature. The samples were rinsed with the solvent, blown dry with argon, and used immediately for the TPD experiments. The quality of the SAMs was verified by contact angle goniometry, X-ray photoelectron spectroscopy, and X-ray absorption spectroscopy.[27]

TPD experiments were performed in a dedicated UHV chamber with a base pressure of $\sim 3 \times 10^{-10}$ mbar. Instead of $H_2O$, $D_2O$ was used to distinguish from background $H_2O$ contribution; the temperature of the sample was kept at 110–115 K during the dosing. The dose was controlled manually by adjusting the leak valve and keeping the $D_2O$ pressure at a constant value of $\sim 1.3 \times 10^{-8}$ mbar. The dose was varied from 0.5 to 8 L and calculated by multiplication of the $D_2O$ pressure

with the dosing time; note that 8 L was just an arbitrary choice for the maximum dose for the given experiments, which was not related to any saturation effects or technical constraints. After the dosing, we waited for ~5 min for stabilization of the base pressure before starting the TPD experiment. The dosing process was additionally controlled by XPS (in another UHV chamber), with the thickness of the $D_2O$ adsorbate films being derived.[27] The TPD measurements were carried out using a linear heating ramp of 0.2–1.0 K $s^{-1}$ but most systematic experiments were performed at 0.5 K $s^{-1}$. The samples (*ca.* 9 mm × 9 mm; 0.5 mm thick) were mounted on a commercial sample holder (PTS 1200 EB/C-K Mo, Prevac, Poland) with electron beam heating. The temperature of the samples was measured by a Ni–CrNi thermoelement, spot welded to the supporting Mo disk (10 mm in diameter), on which, pressed by three stripes, the sample was mounted with good, full-area thermal contact to the disk and touching the thermoelement. The temperature was controlled by the HEAT-2 unit (Prevac, Poland). Quadrex 200 (Inficon) QMS spectrometer with a Feulner cup was used, which allowed to suppress the desorption signal from the sample holder and the parts of the UHV chamber. The signal of the spectrometer was calibrated by integration of the TPD spectra; the integral intensity of the QMS signal over the temperature ramp exhibited a linear dependence on the $D_2O$ dose (see Fig. S1 in the ESI†). A similar coverage *vs.* dose relation was also observed in the complementary spectroscopic experiments.[27]

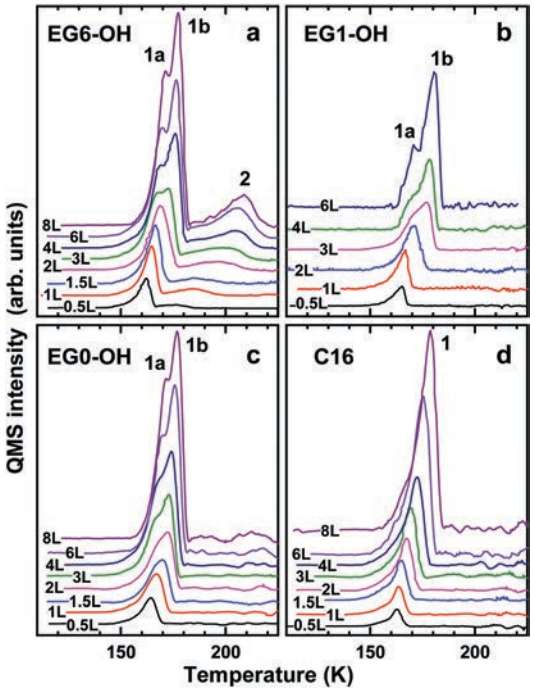


Fig. 2 TPD traces for various doses of $D_2O$ deposited at ~110 K onto the surface of the EG6 OH (a), EG1 OH (b), EG0 OH (c), and C16 (d) SAMs. The heating rate was set to 0.5 K $s^{-1}$. The $D_2O$ doses are marked at the respective curves. Individual desorption peaks and their components are marked by numbers (see text for details).

## Results and discussion

Whereas the wetting properties of the EG*n*–OH SAMs are close to those of the EG0-OH monolayer, their OEG part has a hydrogel character, so that, according to our initial expectations, adsorption of $D_2O$ could not only occur onto the SAM surface (termed below as the "wetting phase") but also inside the OEG part (termed below as the "hydration phase"), with increasing extent for larger *n*. Moreover, looking at the partly hydrogel EG*n*–OH SAMs as a sponge, one can expect that the formation of the hydration phase could occur before the growth of the wetting phase.

However, the observed behavior turned out to be entirely different as shown by representative TPD traces in Fig. 2. At low coverages, the traces for the EG*n*–OH SAMs do not show any significant dependence on *n* and are very similar to that of the EG0–OH film, indicative of formation of the wetting phase only. All these traces exhibit a single desorption peak (**1**) with a maximum at $T \approx 162$–164 K at a dose of 0.5 L, shifting to higher temperatures with increasing $D_2O$ coverage. However, in the EG*n*–OH ($n \geq 3$) traces, there is a weak additional peak at higher temperature (**2**), which, however, is completely absent for the EG1–OH and EG0–OH case, indicative of its "belonging" to the EG*n* part as far as *n* is sufficiently large (see Fig. S2 in the ESI,† for the EG3–OH and EG5–OH data). This peak (**2**), existing also for EG3–OMe (see Fig. S3 in the ESI†), evolves with increasing $D_2O$ coverage and shifts to higher temperatures, along with the main peak (**1**) which also gains in intensity, showing overall typical zero-order desorption behavior. At the same time, starting from a $D_2O$ dose of 3–4 L, the latter peak "splits" to some extent, exhibiting a shoulder at the low temperature side (**1a**), which becomes more pronounced with increasing coverage. Interestingly, such a shoulder is not observed in the C16 trace, which, in agreement with the literature data,[20] exhibits a single desorption peak (**1**), with the maximum at $T \approx 161$ K at a dose of 0.5 L, shifting to higher temperatures with increasing $D_2O$ coverage.

Generally, the TPD traces are described by the Wigner–Polanyi equation

$$-\mathrm{d}\theta_i/\mathrm{d}t = \nu_x \theta_i^x \exp(-E_\mathrm{d}/RT) \quad (1)$$

where $\theta_i$ is the coverage of species *i*, $\nu$ the pre-exponential or frequency factor, $E_\mathrm{d}$ the desorption energy, and *x* the order of desorption.[28,29] Taking a logarithm from both parts of this equation, one gets

$$\ln(-\mathrm{d}\theta_i/\mathrm{d}t) = \ln(\nu_x\, \theta_i^x) - E_\mathrm{d}/RT \quad (2)$$

Following this equation, the original TPD traces in Fig. 2 were replotted in the $\ln(-\mathrm{d}\theta/\mathrm{d}t)$ *vs.* $1000/T$ fashion as shown in Fig. 3 for few representative samples. The modified traces exhibit consistent linear behavior at their low temperature side, corresponding to the leading edge of the joint peak **1** and the respective $E_\mathrm{d}/RT$ term in eqn (2).

Significantly, the slope of the linear part is independent of the coverage, indicative of the persistent desorption energy,

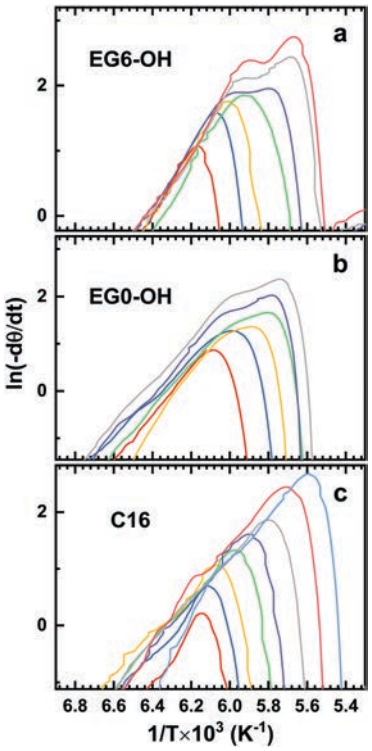


Fig. 3 ln(−dθ/dt) *vs.* 1000/*T* representations of the TPD traces for the EG6 OH (a), EG0 OH (b), and C16 (c) SAMs (analogous traces were drawn for all systems studied). The abscissa scale is reversed for better compar ison to the original traces (Fig. 2), following the approach of ref. 30 and 31. The traces for the different $D_2O$ coverages, corresponding to specific doses, are drawn by the different colors. The traces are shifted along the *x* axis to highlight that the slope at the low temperature side is nearly independent of the coverage.

which can then be calculated. Another important moment is the nearly identical slopes for the EG6–OH and EG0–OH traces (and the other EG*n*–OH monolayers as well), suggesting similar $E_d$ values for all these films. At the same time, the C16 traces in Fig. 3 show a smaller slope compared to those for EG6–OH and EG0–OH, corresponding to a lower desorption energy. Taking the most reliable (in our opinion) literature value for C16/Au, 9.8 kcal mol$^{-1}$,[20] as a reference, we calculated then the desorption energies corresponding to the peak **1** in all other systems of the present study and compiled them in Table 1. Significantly, the $E_d$ values for all –OH terminated SAMs were found to be larger than that for C16/Au but close to each other, being within the 10.7–10.9 kcal mol$^{-1}$ range, while the $E_d$ value for the EG6–OMe SAM is nearly identical to that of C16/Au.

Complementary to the above evaluation, so called complete analysis[28] was performed, relying on the $\theta$ *vs.* $T$ curves obtained by the integration of the TPD traces. Such curves are shown in Fig. 4a and b for the EG6–OH and EG0–OH SAMs, representative of all other systems of the present study. The EG0–OH curves correspond to the joint contribution of the sub-peaks **1a** and **1b**, with the partial contributions being hardly traceable (see Fig. 2). The EG6–OH curves exhibit similar behavior, showing in addition a clear contribution of the peak **2** at high temperatures, appearing as an additional step. Setting the specific coverages to address either the peaks **1** or **2** and getting the temperatures and $-d\theta/dt$ values corresponding to these coverages ($-d\theta/dt$ from the original TPD traces; Fig. 2), we created $\ln(-d\theta/dt)$ *vs.* $1/T$ plots, such as those shown in Fig. 4c. In accordance with eqn (2) these plots represent linear functions with the slopes giving the desorption energies corresponding to the peaks **1** and **2** in the original TPD traces (Fig. 2).

Table 1 Desorption energies (kcal mol$^{-1}$) corresponding to the peak **1** (wetting phase), calculated either from the ln(−dθ/dt) *vs.* 1000/*T* repre sentations of the TPD traces (direct analysis) or by the complete analysis (see below). The error bars of the $E_d$ values were estimated at ±3% for the direct analysis and at ±5% for the complete analysis

| SAM | C16 | EG0 OH | EG1 OH | EG3 OH | EG5 OH | EG6 OH | EG6 OMe |
|---|---|---|---|---|---|---|---|
| Direct analysis | 9.8 | 10.9 | 10.9 | 10.8 | 10.9 | 10.7 | 9.8 |
| Complete analysis | 9.8 | 10.5 | 10.5 | 10.3 | 10.4 | 10.5 | 9.9 |

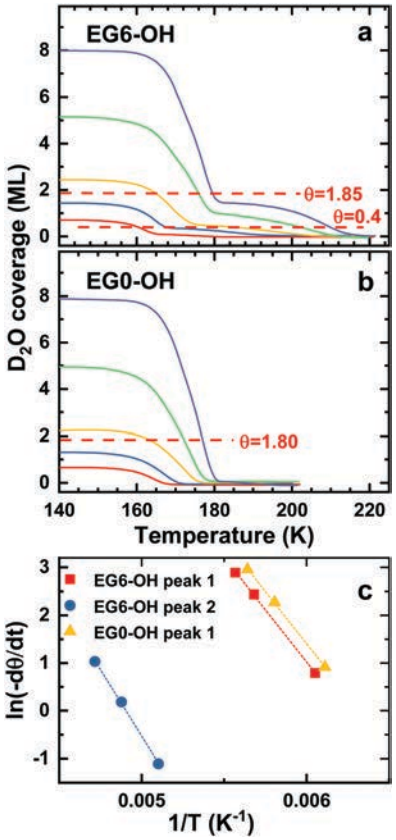


Fig. 4 $\theta$ *vs.* $T$ plots for the EG6 OH (a) and EG0 OH (b) SAMs (analogous plots were drawn for all systems studied) as well as respective $\ln(-d\theta/dt)$ *vs.* $1/T$ plots derived within the complete analysis procedure (c). The setting points for this analysis are marked by the dashed lines in a and b; the respective $\theta$ values are given. The traces for the different $D_2O$ coverages, corresponding to specific doses, are drawn by the different colors. The slope of the linear function corresponding to the peak **2** in (c) is larger than the nearly identical slopes of these functions corresponding to the peak **1**, suggesting a higher $E_d$ value for the peak **2**.

Taking again the literature value for C16/Au, 9.8 kcal mol$^{-1}$,[20] as a reference, we calculated the respective $E_d$ values for the other SAMs and compiled them in Table 1, visualizing additionally in Fig. 5. The results for the peak **1** are very close to those obtained by the analysis of the TPD traces in Fig. 3 (see Table 1). This peak represents obviously the wetting phase, exhibiting similar behavior and similar $E_d$ values for all EG*n*–OH SAMs (including $n = 0$) having the same terminal hydrophilic –OH group. The derived $E_d$ values of 10.3–10.5 kcal mol$^{-1}$ are quite close to the heat of sublimation of ice (11.5 kcal mol$^{-1}$) and to the $E_d$ values reported before for the –OH and –COOH terminated AT SAMs (10.0 and 10.05–11.95 kcal mol$^{-1}$, respectively).[20,23] The derived desorption energy for the EG–OMe film ($\sim$9.9 kcal mol$^{-1}$) is nearly identical to that of C16/Au, as expected in view of the same terminal group (methyl).

As to the peak **2**, a reliable $E_d$ value of *ca.* 12.4 $\pm$ 0.5 kcal mol$^{-1}$ could only be obtained for the EG6–OH SAM, as illustrated in Fig. 4a and c. Since the appearance and intensity of this peak correlates with the OEG termination and the length of the OEG group, it is obviously representative of the hydration phase. Higher desorption temperature corresponding to this peak is indicative of a stronger bond,[32] as this is, *e.g.*, assumed for COOH-terminated monolayer surfaces.[22,23] The respective desorption energy is indeed higher than that for the wetting phase, which can be associated with the formation of suitable conformers of the OEG strands, resulting in effective ''trapping'' of $D_2O$ molecules and dimers.[6,12] A quite broad character of peak **2** reflects probably a certain distribution of bonding configurations for $D_2O$ molecules in the OEG matrix, relying on a broad variety of different conformers. Interestingly, upon the exposure of the EG*n*–OH SAMs to $D_2O$, the adsorption occurs predominantly to the wetting phase, with only a minor involvement of the hydration phase (if at all). This is indicative of a certain activation barrier for the latter phase, which hinders a direct adsorption of $D_2O$ molecules inside the OEG matrix and their diffusion from the wetting to hydration phase. The latter process can however be promoted by temperature as illustrated by the example of the EG6–OH SAM in Fig. 6 where two series of the TPD traces acquired with the standard temperature ramp (Fig. 6a) and the ramp containing an intermediate annealing step at a temperature below the main desorption peak (Fig. 6b), are presented (analogous experiments, with the same outcome, were also performed for the EG3–OH and EG3–OMe monolayers). As seen by comparison of the respective traces for the same $D_2O$ doses, the relative contribution of the hydration phase increased considerably upon the annealing. Significantly, the latter procedure did not change the integral intensity of the TPD signal, as illustrated by Fig. 6c, which suggests that the contribution of the hydration phase increased exclusively on the expense of the wetting phase, presumably, by the temperature-promoted diffusion (as suggested above).

Note that along with the proposed existence of the specific energetic barrier for the formation of the hydration phase, which is a thermodynamic factor, formation and decomposition of this phase may be affected by kinetic reasons as well. In particular, hydration may require rearrangement of the OEG chains, which may slow down hydration for entropic reasons and may give rise to very low pre-factors in the kinetics.

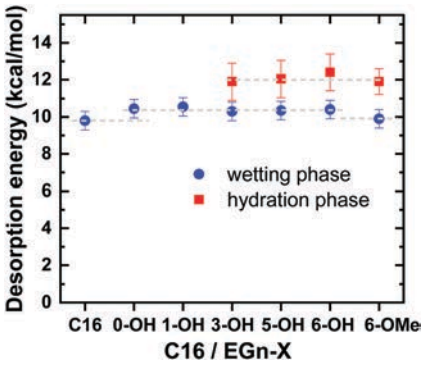


Fig. 5 Desorption energies corresponding to the peaks **1** (blue circles) and **2** (red squares) in the original TPD traces, representative of the wetting and hydration phases, respectively (see text for details). The horizontal gray dashed lines are guides for the eyes. The different error bars for the different $E_d$ values are related to the accuracy of the specific approaches used for their calculations (see text for details).

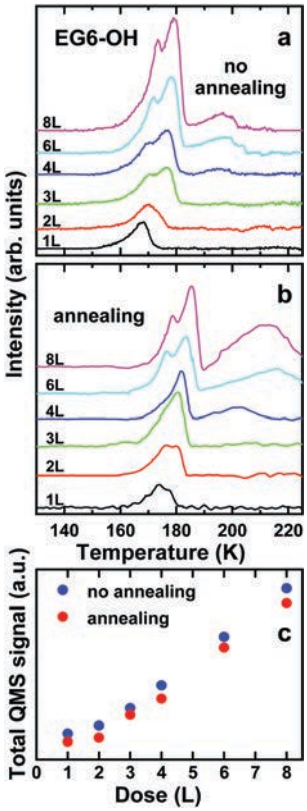


Fig. 6 (a) TPD traces for various doses of $D_2O$ deposited at $\sim$110 K onto the surface of the EG6 OMe SAM; the heating rate was 0.3 K s$^{-1}$; (b) Analogous TPD traces with intermediate ''annealing'' of the EG6 OMe SAM at 140 K for 10 min. (c) Integral intensity of the TPD signal for the temperature ramp with (blue squares) and without (red circles) the annealing step. The $D_2O$ doses are marked at the respective curves. The observed slight nonlinearity of the total QMS signal as a function of dose was only observed in this particular experiment and doesn't affect its implications.

Whereas the $E_d$ values for the hydration phase in the EG3–OH, EG5–OH and EG6–OMe SAMs could not be reliably derived from the complete analysis, they can be coarsely evaluated on the basis of the positions of the respective desorption peak, $T_p$, using, *e.g.*, a formula obtained by Redhead for the first-order desorption

$$E_d = RT_p[\ln(\nu T_p/\beta - 3.64)] \quad (3)$$

where $R$ is the gas constant, $\nu$ the frequency factor, and $\beta$ the heating rate.[33] Taking the $E_d$ value derived within the complete analysis for the EG6–OH film (12.4 kcal mol$^{-1}$) as a reference and the respective $T_p$ from the experimental data, the frequency factor could be calculated and, subsequently, based on the respective $T_p$ values, the $E_d$ values for the EG3–OH, EG5–OH and EG6–OMe SAMs could be estimated at 11.9–12.1 $\pm$ 0.5 kcal mol$^{-1}$. They are visualized in Fig. 5 and can be considered as very tentative only in view of the non-strict character of the given evaluation procedure.

The question left so far in the discussion of the experimental data is the ''splitting'' of the most prominent desorption peak **1** in the TPD traces of the EG*n*–OH and EG*n*–OMe films. The contributions of the individual components, **1a** and **1b** (see Fig. 2), could regretfully not be clearly separated and evaluated in terms of $E_d$. The nature of this ''splitting'', mentioned shortly in previous publications,[20,21] can, however, be considered. Special features of this ''splitting'' are: (i) its appearance for hydrophilic surfaces only, (ii) its appearance beginning with high coverages, and (iii) its appearance in the temperature range corresponding to the structural transformation from amorphous to polycrystalline ice (according to ref. 26). Note that, according to the literature data,[26] pinning of $D_2O$ to OH impedes such structural transformation at lower temperatures but the substrate effect extends up to 5 ML only for the OH-terminated surfaces. Note also that this structural change can be accompanied by a partial transformation from the two-dimensional cluster morphology, typical of hydrophilic surfaces, to drop-like morphology,[24] involving probably only the topmost part of the two-dimensional ice clusters. Therefore, according to the above considerations, the appearance of two distinct peaks within the entire desorption peak **1** can stem from either structural or morphological effects or their combination. The former effects can include appearance of a different structural phase in the topmost part of the two-dimensional ice film. The latter effects can involve formation of drop-like clusters on the surface of this film, with somewhat different energetics as compared to the film itself.

We see, however, the ''splitting'' of the peak **1** as a less important feature of the TPD traces, whereas the peak **2**, observed for the first time (to the best of our knowledge) and representing the hydration phase in the OEG-terminated SAMs is of primary importance. This peak, which was recorded neither for the reference C16 and EG0–OH SAMs nor for the EG1–OH monolayers, appears first in the TPD traces for the EG3–OH films and gains in intensity at going to the EG5–OH and further to EG6–OH SAMs. This behavior correlates well with the biorepulsivity of the respective surfaces,[7,9] linking, thus, the latter property to the existence and ''amount'' of the hydration phase.

## Conclusions

Interaction of water ($D_2O$) with a series of OH- and $CH_3$-terminated, OEG-substituted AT SAMs on Au(111) was studied by TPD. The length of the OEG strand was varied and the behavior of the OEG-substituted films was compared to that of representative OH-terminated and non-substituted AT SAMs on the same substrate. Whereas these reference SAMs exclusively exhibited formation of conventional ice overlayer, termed as a wetting phase, upon the $D_2O$ adsorption, the TPD traces of the OEG-substituted monolayers suggested formation of an additional, hydration phase, corresponding to the adsorption of $D_2O$ into the OEG matrix. The relative weight of this phase correlated with the length of the OEG strand and the respective desorption energy, 12.4 kcal mol$^{-1}$, turned out to be significantly higher than that for the wetting phase ($\sim$10.4 kcal mol$^{-1}$). The adsorption of $D_2O$ into the OEG matrix was found to occur over an activation barrier, presumably by temperature-promoted diffusion from the wetting phase, with the latter process being additionally enforced by a pre-desorption annealing. Apart from this process, the wetting phase for the OH-terminated OEG-AT SAMs exhibited similar behavior and was characterized by a similar desorption energy as that for the reference, OH-terminated AT monolayer. In contrast, the desorption energy of the wetting phase for the $CH_3$-terminated OEG-AT SAMs was noticeably lower (9.8–9.9 kcal mol$^{-1}$) and close to that for the reference, non-substituted AT monolayer, having the same termination.

The formation of a hydration phase with a comparably high characteristic energy for the OEG-substituted AT SAMs can be of importance in context of well-known biorepulsion behavior of these systems, supporting their special character in relation to their interaction with water, frequently seen as a key element for bioinertness.

## Conflicts of interest

There are no conflicts to declare.

## Acknowledgements

This work has been supported by the German Research Foundation (DFG; projects ZH 63/21-1 and NE 984/2-1).

## References

1 S. I. Jeon, J. H. Lee, J. D. Andrade and P. G. D. Gennes, Protein-surface interactions in the presence of polyethylene oxide: I. Simplified theory, *J. Colloid Interface Sci.*, 1991, **142**, 149–158.

2 K. L. Prime and G. M. Whitesides, Self-assembled organic monolayers: model systems for studying adsorption of proteins at surfaces, *Science*, 1991, **252**, 1164–1167.

3 *Polyethylene glycol chemistry: Biotechnical and ciomedical applications*, ed. J. M. Harris, Plenum Press, New York, 1992.

4 P. Harder, M. Grunze, R. Dahint, G. M. Whitesides and P. E. Laibinis, Molecular conformation in oligo(ethylene glycol)-terminated self-assembled monolayers on gold and silver surfaces determines their ability to resist protein adsorption, *J. Phys. Chem. B*, 1998, **102**, 426–436.

5 S. Herrwerth, W. Eck, S. Reinhardt and M. Grunze, Factors that determine the protein resistance of oligoether self-assembled monolayers – internal hydrophilicity, terminal hydrophilicity, and lateral packing density, *J. Am. Chem. Soc.*, 2003, **125**, 9359–9366.

6 A. Rosenhahn, S. Schilp, H. J. Kreuzer and M. Grunze, The role of ''inert'' surface chemistry in marine biofouling prevention, *Phys. Chem. Chem. Phys.*, 2010, **12**, 4275–4286.

7 S. Schilp, A. Rosenhahn, M. E. Pettitt, J. Bowen, M. E. Callow, J. A. Callow and M. Grunze, Physicochemical properties of (ethylene glycol)-containing self-assembled monolayers relevant for protein and algal cell resistance, *Langmuir*, 2009, **25**, 10077–10082.

8 R. Valiokas, L. Malysheva, A. Onipko, H.-H. Leed, Z. Ruzele, S. Svedhem, S. C. T. Svensson, U. Gelius and B. Liedberg, On the quality and structural characteristics of oligo(ethylene glycol) assemblies on gold: an experimental and theoretical study, *J. Electron Spectrosc. Relat. Phenom.*, 2009, **172**, 9–20.

9 C. Christophis, M. Grunze and A. Rosenhahn, Quantification of the adhesion strength of fibroblast cells on ethylene glycol terminated self-assembled monolayers by a microfluidic shear force assay, *Phys. Chem. Chem. Phys.*, 2010, **12**, 4498–4504.

10 T. Hayashi, Y. Tanaka, Y. Koide, M. Tanaka and M. Hara, Mechanism underlying bioinertness of self-assembled monolayers of oligo(ethyleneglycol)-terminated alkanethiols on gold: protein adsorption, platelet adhesion, and surface forces, *Phys. Chem. Chem. Phys.*, 2012, **14**, 10196–10206.

11 S. I. Jeon and J. D. Andrade, Protein-surface interactions in the presence of polyethylene oxide: II. Effect of protein size, *J. Colloid Interface Sci.*, 1991, **142**, 159–166.

12 R. L. C. Wang, H. J. Kreuzer and M. Grunze, Molecular conformation and solvation of oligo(ethylene glycol)-terminated self-assembled monolayers and their resistance to protein adsorption, *J. Phys. Chem. B*, 1997, **101**, 9767–9773.

13 Y. H. M. Chan, R. Schweiss, C. Werner and M. Grunze, Electrokinetic characterization of oligo- and poly(ethylene glycol)-terminated self-assembled monolayers on gold and glass surfaces, *Langmuir*, 2003, **19**, 7380–7385.

14 A. J. Pertsin, T. Hayashi and M. Grunze, Grand canonical Monte Carlo simulations of the hydration interaction between oligo(ethylene glycol)-terminated alkanethiol self-assembled monolayers, *J. Phys. Chem. B*, 2002, **106**, 12274–12281.

15 D. Schwendel, T. Hayashi, R. Dahint, A. Pertsin, M. Grunze, R. Steitz and F. Schreiber, Interaction of water with self-assembled monolayers: neutron reflectivity measurements of the water density in the interface region, *Langmuir*, 2003, **19**, 2284–2293.

16 J.-M. Zheng, W.-C. Chin, E. Knijniak, E. Knijniak Jr. and G. H. Pollack, Surfaces and interfacial water: evidence that hydrophilic surfaces have long-range impact, *Adv. Colloid Interface Sci.*, 2006, **127**, 19–27.

17 T. Sekine, S. Asatyas, C. Sato, S. Morita, M. Tanaka and T. Hayashi, Surface force and vibrational spectroscopic analyses of interfacial water molecules in the vicinity of methoxy-tri(ethylene glycol)-terminated monolayers: mechanisms underlying the effect of lateral packing density on bioinertness, *J. Biomater. Sci., Polym. Ed.*, 2017, **28**, 1231–1243.

18 D. J. Vanderah, J. Arsenault, H. La, R. S. Gates, V. Silin and C. W. Meuse, Structural variations and ordering conditions for the self-assembled monolayers of $HS(CH_2CH_2O)_{3\text{-}6}CH_3$, *Langmuir*, 2003, **19**, 3752–3756.

19 N. M. Pawlowska, H. Fritzsche, C. Blaszykowski, S. Sheikh, M. Vezvaie and M. Thompson, Probing the hydration of ultrathin antifouling organosilane adlayers using neutron reflectometry, *Langmuir*, 2014, **30**, 1199–1203.

20 I. Engquist, I. Lundström and B. Liedberg, Temperature-programmed desorption and infrared studies of $D_20$ ice on self-assembled alkanethiolate monolayers: influence of substrate wettability, *J. Phys. Chem.*, 1995, **99**, 12257–12267.

21 I. Engquist, M. Listelius and B. Liedberg, Microscopic wettability of ester- and acetate-terminated self-assembled monolayers, *Langmuir*, 1997, **13**, 4003–4012.

22 R. L. Grimm, N. M. Barrentine, C. J. H. Knox and J. C. Hemminger, D2O water interaction with mixed alkane thiol monolayers of tuned hydrophobic and hydrophilic character, *J. Phys. Chem. C*, 2008, **112**, 890–894.

23 R. L. Grimm, D. J. Tobias and J. C. Hemminger, $D_2O$ water interaction with textured carboxylic acid-terminated monolayer surfaces characterized by temperature-programmed desorption and molecular dynamics, *J. Phys. Chem. C*, 2010, **114**, 1570–1579.

24 I. Engquist, M. Listelius and B. Liedberg,, Hydrogen bond interaction between self-assembled monolayers and adsorbed water molecules and its implications for cluster formation, *J. Phys. Chem.*, 1995, **99**, 14198–14200.

25 I. Engquist and B. Liedberg, $D_2O$ Ice on controlled wettability self-assembled alkanethiolate monolayers: cluster formation and substrate-adsorbate interaction, *J. Phys. Chem.*, 1996, **100**, 20089–20096.

26 I. Engquist, A. N. Parikh, D. L. Allara, I. Lundström and B. Liedberg, Infrared characterization of amorphous and polycrystalline $D_2O$ ice on controlled wettability self-assembled alkanethiolate monolayers, *J. Chem. Phys.*, 1997, **106**, 3038–3048.

27 M. Sayin, A. Nefedov and M. Zharnikov, Spectroscopic study of water adsorption and desorption on/from oligo(ethylene glycol)-substituted alkanethiolate self-assembled monolayers, *J. Phys. Chem. C*, 2018, **122**, 10918–10928.

28 D. A. King, Thermal desorption from metal surfaces: A Review, *Surf. Sci.*, 1975, **47**, 384–402.

29 A. M. de Jong and J. W. Niemantsverdriet, Thermal desorption analysis: comparative test of ten commonly applied procedures, *Surf. Sci.*, 1990, **233**, 355–365.
30 B. Lehner, M. Hohage and P. Zeppenfeld, The influence of weak adsorbate–adsorbate interactions on desorption, *Chem. Phys. Lett.*, 2003, **369**, 275–280.
31 M. Roos, D. Künzel, B. Uhl, H.-H. Huang, O. B. Alves, H. E. Hoster, A. Gross and R. J. Behm, Hierarchical interactions and their influence upon the adsorption of organic molecules on a graphene film, *J. Am. Chem. Soc.*, 2011, **133**, 9208–9211.
32 N. S. Faradzhev, K. L. Kostov, P. Feulner, T. E. Madey and D. Menzel, Stability of water monolayers on Ru(0001): thermal and electronically induced dissociation, *Chem. Phys. Lett.*, 2005, **415**, 165–171.
33 P. A. Redhead, Thermal desorption of gases, *Vacuum*, 1962, **12**, 203–211.